Received: 4 April 2023 | Revised: 25 May 2023 | Accepted: 20 June 2023

DOI: 10.1002/ppap.202300071

RESEARCH ARTICLE

PLASMA PROCESSES AND POLYMERS

Structure of plasma deposited acrylic acid-allyl alcohol copolymers

Alaa Fahmy[1,2] | **Hassan Omar**[2] | **Paulina Szymoniak**[2] | **Andreas Schönhals**[2] | **Jörg Florian Friedrich**[3]

[1]Department of Chemistry, Faculty of Science, Al-Azhar University, Cairo, Egypt

[2]Materialchemie, Bundesanstalt für Materialforschung und -prüfung (BAM), Berlin, Germany

[3]Werkstoffwissenschaften, Polymertechnik und Polymerphysik, Technische Universität Berlin, Berlin, Germany

Correspondence
Andreas Schönhals, Materialchemie, Bundesanstalt für Materialforschung und -prüfung (BAM), Unter den Eichen 87, 12205 Berlin, Germany.
Email: andreas.schoenhals@bam.de

Jörg Florian Friedrich, Polymertechnik und Polymerphysik, Technische Universität Berlin, Ernst-Reuter-Platz 1, 10587 Berlin, Germany.
Email: joerg.florian.friedrich@gmx.de

Abstract

Copolymer thin films with two types of functional groups have excellent performance as sensors, for example. The formation and deposition of allyl alcohol-acrylic acid copolymer films by pulsed high frequency plasma is a complex process. As usual, the chemical composition of the top surface of the films was investigated by XPS and FTIR measurements. Furthermore, contact angle measurements with water were used to characterise the hydrophilicity and wettability of the polymer films. After plasma deposition, a significant decrease in functional groups (OH and COOH) was observed compared to the classically copolymerised equivalent. The remaining functional groups, i.e. the majority of these groups, were sufficient for application as sensor layers. Segmental mobility and conductivity, important for sensor applications, were analysed by broadband dielectric spectroscopy.

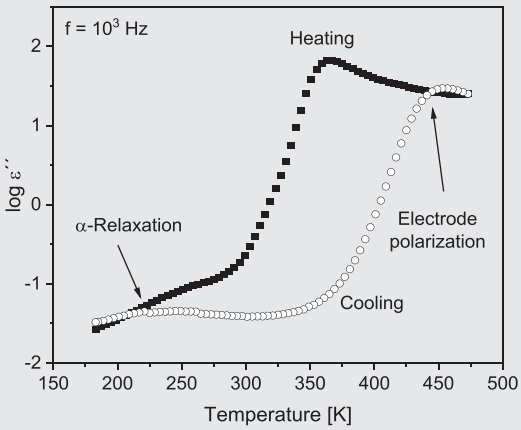

KEYWORDS

acrylic acid, allyl alcohol, copolymer thin film, plasma deposition, segmental mobility

1 | INTRODUCTION

The control of the pH value of chemical, bio-chemical and environmental reactions in aqueous solution is important.[1] For example, enzyme-catalysed chemical reactions, biochemical inactivation or protein denaturation depend on pH. Unwanted changes in pH can disrupt cell function. Continuous pH control is therefore essential.[2]

Known pH sensors are based on polymer gels.[3] One type has been made using poly (vinyl alcohol) (PVA) and poly (acrylic acid) (PAA). The function of such a sensor is simple. The gel swells as the pH rises or falls. This is read

by a detector with the gel placed in a special membrane.[4] The diaphragm is deformed by changing the pH value.[5] Another example of the application of alternative plasma polymerised copolymer layers is their use as biosensors. The problem in producing suitable biosensing devices is to achieve stable chemical binding to covalently immobilised bioreceptors (e.g., antibody capture) such as single-stranded DNA (ss-DNA). They must bind selectively to a target by matching an antigen or oligonucleotide sequence (DNA or RNA fragment) of interest for bio-diagnostics.[6] Carboxylic (COOH) groups are particularly suitable for biosensing applications because they form amide (peptide) bridges by reacting with the amino groups of biomolecules (e.g., receptor antibodies). This requires activation energy and removal of water. Such binding has been demonstrated using plasma-deposited copolymer layers of allylamine and allyl alcohol to immobilise both human dermal fibroblasts and E. col.[7,8]

The focus here is on the measurement of pH. A review of the various methods used to date to control pH in wastewater or biological systems summarises most of the techniques used.[9] This paper evaluates the general applicability of plasma polymers as sensors and, in particular, plasma copolymers for pH monitoring. Of particular interest are layers with different functional groups that can be combined to form copolymer-like macromolecules.[10] The deposition of such plasma-polymerised copolymers as pH-sensitive coatings is a powerful alternative to other coating processes because it results in pinhole-free and well-adhered ultra-thin coatings with adjustable composition and thickness and some stability. Plasma-induced copolymerisation of two comonomers is well suited for easily varying the composition of the polymer. Such a copolymerisation process can also be used to vary the density of functional groups in the deposited layer by mixing one comonomer with the functional group in focus and another without any functional group.[11] Another aspect is the "mixing" of two monomers with different functional groups for copolymerisation to obtain a bifunctional copolymer that can be used for different purposes, such as immobilisation of species,[6] production of pervaporation membranes,[12] or the use in (plasma-less) electrospinning or electrospray deposition.[13,14]

In this work, acrylic acid (AA) and allyl alcohol (AAl) monomers were chosen because, as mentioned above, the COOH and OH groups are suitable for biosensing applications. In general, there are two types of interactions between the AA-Al segments: (1) copolymers with covalent bonds between the AA-Al units or (2) homopolymers with hydrogen bonds between the –COOH and –OH groups. To the best of our knowledge, the copolymerisation parameters of the AA-AAl comonomer pair have not been reported in the literature. Four methods are available to estimate copolymerisation parameters, the Mayo–Lewis, Fineman-Ross and Kelen-Tüdös approaches and the Alfred-Price Q,e scheme.[14] However, when comparing similar pairs of comonomers, radical AA-Al copolymerisation may be preferred to homopolymerisation due to the polar nature of the comonomer. The AA molecule is characterised by negative inductive and mesomeric effects in the copolymerisation process. AAl shows positive mesomeric effects combined with slightly negative inductive effects. This would indicate a preferential formation of an alternating copolymer –[CH_2–CH(COOH)–CH_2–CH(CH_2–OH)]–. However, conventional free radical polymerisation of allyl alcohol is limited by self-inhibition due to degradative chain transfer.[15] Therefore, high molecular weight products should not normally be obtained.

Plasma copolymerisation does not follow all the classical chemical rules due to the significant excess energy introduced by the plasma. Thus, in addition to the classical copolymerisation process, partial fragmentation of monomers, precursors or gases and their recombination into a randomly formed cross-linked conglomerate must be expected as a side reaction.[16] Polymers with longer chains with regular sequences may also be formed under low pressure conditions, primarily within the irregular polymer conglomerate. However, the intense irradiation of the plasma can further randomise the possibly formed classically polymer sequences. There is no known result in the literature that clearly shows the existence of a band at 721–726 cm^{-1} in IR spectra characteristic of intact $[CH_2]_n$ sequences with $n \geq 4$.[17]

From an analytical point of view, it is difficult to confirm regular polymer structures and the preservation of the original functional groups. However, the amount of OH and COOH groups can be accurately estimated by X-ray photoelectron spectroscopy (XPS) and infrared spectroscopy (IR). Here, these and additional methods were used to investigate the general applicability of plasma polymerisation for the synthesis of copolymers for pH sensing.

2 | EXPERIMENTAL SECTION

2.1 | Materials

Polyethylene (PE) foils and thin layers of aluminium (Al) (thickness 150 nm) evaporated on glass slides were used as substrates for plasma deposition of the copolymers.

PE with a thickness of 40 μm was obtained from Alkor Folien GmbH, Germany. Al wires of 99.95% purity were supplied by Goodfellow. Microscope slides were used after careful cleaning. Acrylic acid ($CH_2=CH–COOH$) (»99% purity) was purchased from Fluka. Allyl alcohol ($CH_2=CH–CH_2–OH$) of 99% purity, trifluroacetic anhydride (99.5% purity) and trifluoroethanol were obtained from MERCK, Germany.

2.2 | Film preparation

The plasma polymerisation experiments were carried out in a 50 dm^3 stainless steel reactor (Ilmvac). The reactor was connected to a pulsable radiofrequency generator (RF 13.56 MHz) via a flat RF electrode (5 × 35 cm, steel) and an automatic matching unit. A 10 cm diameter cylinder served as a grounded rotating counter-electrode, mounted 2.5 cm from the driven steel electrode. The rotation (12 rpm) of this earthed electrode increases the deposition area and results in a more homogeneous deposition over this larger area. The effective area of the grounded electrode was approximately 1.5–2 times that of the RF electrode. The monomer vapours were introduced into the reactor through perforated and heated steel tubes located above the substrate attached to the rotating electrode. The monomer dosage was controlled by liquid mass flow controllers (Liqui-Flow®, Bronkhorst) and set at 10 g/h. The pressure was kept constant at 10 Pa by varying the speed of the turbomolecular pump and/or automatically by a butterfly valve (V.A.T.). A quartz microbalance was used to monitor the film thickness and thus the deposition rate. To calculate the thickness of the deposited film, a density of 1 g/cm^3 of the polymer film was assumed. This is a value based on previous experience. The expected differences from the real density caused by variations in the duty cycle should be small (<5%). It is assumed that the density of the deposited layers is not significantly affected by variations in plasma conditions compared to other factors. The duty cycle is defined by

$$DC = \frac{t_{pulse-on}}{t_{pulse-on} + t_{pulse-off}}, \quad (1)$$

where $t_{pulse\text{-}on}$ and $t_{pulse\text{-}off}$ are the time intervals where the plasma power is on or off, respectively. The duty cycle was set to 0.5.

Six layers with different formulated concentrations of acrylic acid and allyl alcohol monomers were deposited on the PE substrate or Al to form polyethylene-poly (acrylic acid) (PE-PAA), polyethylene-poly (acrylic acid)-poly (allyl alcohol) (PE-PAA-Al) copolymers with the following comonomer ratios 4:0, 3:1, 2.1, 1:1, 1:2, 1:3 and 0:4 molar ratio of AA:AAl (100%, 75%, 67%, 50%, 33%, 25% and 0%). Once the copolymer films were produced, they were immediately tested.

2.3 | Characterisation of copolymers

2.3.1 | FT-IR

A Nicolet Nexus 8700 FT-IR spectrometer (Nicolet) was used to characterise the chemical composition. The spectrometer was equipped with the appropriate ATR accessory (Diamond Golden Gate, 1 reflection, Nicolet). The spectra were recorded in the wavenumber range 4000–500 cm^{-1} by accumulating 64 scans with a resolution of 4 cm^{-1}.

2.3.2 | XPS

The surface composition and the types of functional groups of the plasma deposited A/S copolymer films were investigated by XPS by analysing the C1s and O1s peaks. A SAGE 150 spectrometer (Specs) was used for this purpose. It was equipped with a Phoibos 100 MCD-5 hemispherical analyser and a non-monochromatic AlKα radiation source. The pressure in the chamber was approximately 1×10^{-7} Pa. The analyser was positioned at an angle of 18° with respect to the surface normal, where the angle between the axis of the X-ray source and the analyser lenses was 54.9°.

2.3.3 | Derivatization with TFAA and TFE

Derivatised samples were examined by XPS to obtain more information on the amount of OH and COOH groups. These functional groups are chemically converted with materials consisting of heteroatoms (tetrafloroacetic acid and tetrafloroethanol). The quantification of these heteroatoms is analysed by XPS and the number of functional groups per 100 carbon atoms can be found. However, the derivatisation reactions are described in detail in our previous articles, including a discussion of their possible problems and failures.[18,19]

2.3.4 | Contact angle

Water contact angle (CA) measurements were carried out to investigate the wettability of the samples. The

automated CA system G2 (Krüss) was used to perform the measurement by the sessile drop method. The Fowkes, Owens, Wendt and Rabel method, as implemented in the Krüss software, was used for data analysis.[20]

2.3.5 | Broadband dielectric spectroscopy (BDS)

The molecular mobility of the copolymers was studied using BDS. BDS is a tool to investigate different motion processes in a sample, such as configurational rearrangements and segmental fluctuations. For further details see ref.[21] The complex dielectric function $\varepsilon^*(f) = \varepsilon'(f) - i\varepsilon''(f)$ was measured isothermally in a wide range of frequencies from 10^{-1} to 10^6 Hz and temperatures from 173 to 453 K. Here ε' is the real part of the complex dielectric function where ε'' is the corresponding imaginary or loss part. f denotes the frequency and i the imaginary unit. Details of the sample preparation are given in ref.[22] Briefly, an Al strip was deposited on a glass substrate. The sample was then deposited. After deposition, a second Al strip was evaporated perpendicular to the first. The intersection area defines the capacitor in parallel plate geometry.

3 | RESULTS AND DISCUSSION

3.1 | Deposition rate

The first parameter considered was the deposition rate R_{co}. It should be noted that the deposition rate is less indicative of the composition of the copolymer. R_{co} is estimated from the deposition time dependence of the film thickness (see inset Figure 1) and plotted against composition in Figure 1. For high concentrations of AA, the deposition rate shows a plateau up to a composition of about 67%. The plateau value is similar to the deposition rate of acrylic acid RAA.

As the AA concentration decreases, a minimum deposition rate is observed for the 50% monomer composition. The minimum could be due to true copolymerisation, as pure allyl alcohol has a much lower deposition rate (R_{AAl}) than acrylic acid (Figure 1). The polymerisation of AAl is particularly different from that of vinyl monomers due to self-inhibition by degradative chain transfer:

$$\sim CH_2{-}CH{\bullet}(CH_2OH) + CH_2{=}CH(CH_2OH) \rightarrow \sim CH_2{-}CH_2(CH_2OH) + (CH_2{=}{=}CH{-}{=}CH{-}OH).$$

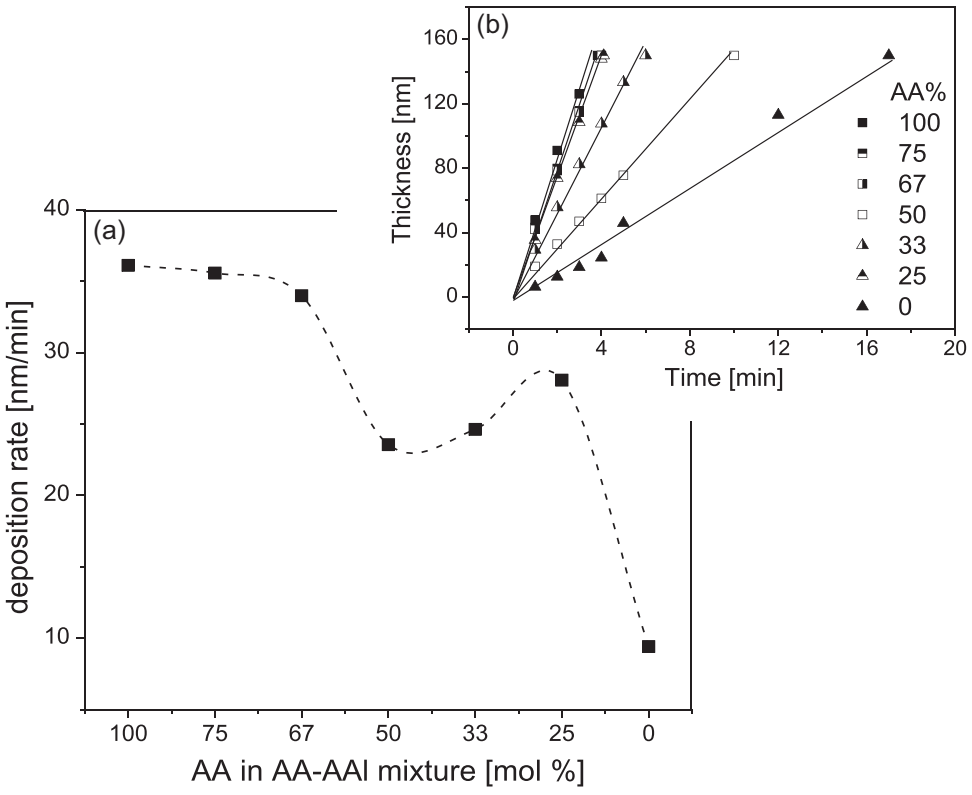

FIGURE 1 Deposition rate in dependence on the molar mixing ratio of comonomers (a). The inset depicts the thickness of the versus the deposition time (b).

The resonance stabilised monomer molecule is too stable to add monomer molecules. Therefore, the polymerisation rate of allyl monomers is only a function of the initiator concentration, which is constantly being generated in the plasma. This has been discussed in detail elsewhere.[19,23] However, the deposition rate decreases for AA ratios 25% > 33% > 50% before an increase is observed at 67%. The H-bonding and condensation processes could be the reasons for this anomalous behaviour. It is well known that the gaseous state is the most active state for a reaction and therefore the reactants react most easily under this condition [i.e., condensation process (–OH + –COOH)]. Both H-bonding and condensation can inhibit the keto-enol form in the AAl structure. Thus, the π bond will be more active and consequently the deposition rate will be increased in the case of a low amount of AA. This behaviour is discussed in more detail in the FTIR section.

3.2 | XPS analysis of copolymers

The composition of the pulsed plasma deposited copolymers was investigated by XPS using a fitting of four components with binding energies of 285.0 eV (aliphatic C–H and C–C bonds), 286.3 eV (C atoms single bonded to O), 287.5 eV (C atoms double bonded to O) and 289.0 eV (C atoms triple bonded to O) (Figure 2) to the C1s peak.

The exceptionally high value of BE = 286.3 eV (OR), in combination with 287.5 (>C=O) and 298.0 eV (COOR), may reflect the post-plasma auto-oxidation of the allyl alcohol plasma polymer on exposure to air. OR and COOR OR and COOR stand for OH and COOH, but take into account the possibility of esterification of these groups under plasma conditions.

To verify the exact nature of these non-specific bonds, post-plasma chemical labelling of the OH groups with trifluoroacetic anhydride (TFAA) and of the COOH groups with trifluoroethanol (TFE) was also performed. The results of the XPS measurements after these derivatisation reactions together with the total oxygen atoms O_{total} (%O/C) are shown in Figure 3.

In the case of derivatisation, the exceptionally high OR concentrations (36 OR/C compared to the theoretical 33 OH/C) are no longer observed. The O_{total} concentration in Figure 3 is much lower than the concentration sum of OH + > CO + COOH in Figure 2, which also indicates all oxygen. Here, it is clear that the derivatisation processes in solvents have removed the extra portion of oxygen by post-plasma auto-oxidation.

The concentration of COOH groups originating from the acrylic acid units in the copolymer decreases with increasing concentration of AAl in the precursor mixture. On the contrary, the concentration of OH groups increases with increasing addition of AAl. It is noteworthy that the decrease of COOH and the increase of OH are not linear. This result indicates a preferential incorporation of acrylic acid into the copolymer at high concentrations of AAl. However, homopolymerisation cannot be excluded. It is therefore assumed that at low concentrations of AAl there is a preferential homopolymerisation of AA and vice versa of AA in the respective precursor mixture. The overall lower concentrations measured after derivatisation of OH and COOH

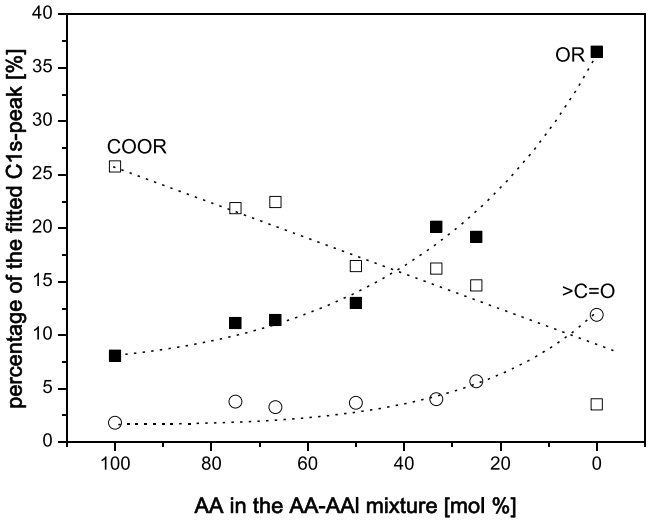

FIGURE 2 Concentration dependence of the components identified from the C1s peak. Lines are guides to the eyes.

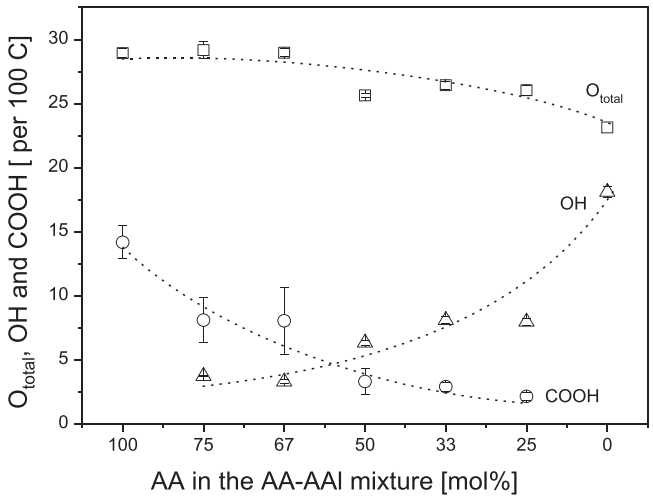

FIGURE 3 Concentration of OH and COOH groups of the deposited copolymers estimated by derivatization and XPS-measurement of the introduced flour concentration as well as O_{total} in dependence on the ratio of comonomers. Lines are guides for the eyes.

compared to the results calculated after XPS peak fitting (Figures 2 and 3) indicate loss by dissolution of autoxidation products and probably some esterification between OH and COOH groups. The derivatisation of COOH groups with trifluoroethanol in the presence of di-tert.-butylcarbodiimide may also have favoured some esterification of COOH from acrylic acid units with those of OH groups introduced with allyl alcohol.

It can be speculated that copolymerisation and homopolymerisation will occur. In the case of acrylic acid, self-condensation is also possible: n $CH_2=CH–COOH \rightarrow –CH_2–CH_2–CO–O–$.

Figure 3 shows that the concentration of OH groups in the copolymer varied from 3% to 8% OH/C and did not exceed 8% OH/C. Only the pure allyl alcohol plasma polymer shows an OH/C content of 18% instead of the theoretically expected 33%. This is also in contrast to the very high peak-fitting result for C–O species with a binding energy of BE = 286.3 eV. An indication of copolymerisation should be the non-linear increase/decrease of OH and COOH in the copolymer. A simple homopolymerisation would show linear behaviour.

As mentioned above, it must also be taken into account that remaining trapped radicals in the plasma polymer can react with oxygen from the ambient air and initiate an auto-oxidation process that also produces post-plasma OH groups. In addition, some additional C–OH, >C=O and COOH groups can be expected from the oxidation reaction: $\geqslant C\bullet + \bullet O\text{-}O\bullet \rightarrow \geqslant C–O–O\bullet \rightarrow \geqslant CO–OH \rightarrow C–OH$, >C=O, COOH.[24]

The O_{total} content estimated by XPS is in the range of 23%–29% O/C of the labelled copolymer and is much lower than the characteristic stoichiometric values expected for allyl alcohol and acrylic acid with 33% O/C. This discrepancy can be explained by dissolution during the labelling processes as mentioned above. In addition, the quenching of the wet-labelling processes also quenches trapped radicals. Any long-term auto-oxidation is thus inhibited.

Acrylic acid tends to release CO or even CO_2, which explains the values of 29% O/C for the concentration range of 100% to 50% acrylic acid in the precursor mixture. The greater loss of oxygen for allyl alcohol on exposure to plasma (Figure 3) has already been explained. For the 50/50 mixture, the corresponding O/C value was only 26%, which is the minimum for all copolymer layers deposited. The labelled OH and COOH groups contribute only 10% O/C for the 50/50 mixture. 16% must be C–O–C, C=O or COOR. Some carbonyls, with a binding energy of about 287.5 eV in the C1s peak, i.e. ketones (>C=O) and aldehydes (CHO), can also be formed by an auto-oxidation process due to contact with air.

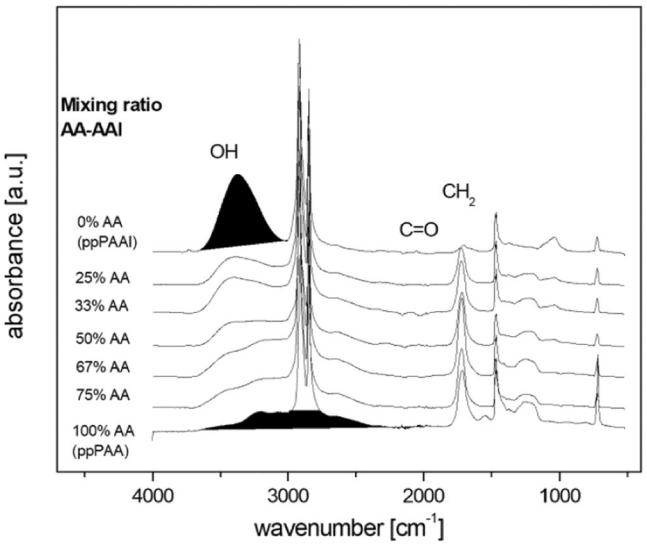

FIGURE 4 Set of IR-ATR spectra of acrylic acid-allyl alcohol copolymers of different comonomer mixtures. IR, infrared spectroscopy.

3.3 | IR-ATR analysis of the copolymers

The IR spectra of the copolymers deposited with different comonomer blend ratios are collected in Figure 4. The spectra of pure poly (allyl alcohol) show a weak C=O stretching band, weaker than expected from the C1s peak fitting analysis shown in Figure 2. This behaviour can be explained by the differences in the information depth of the two techniques, which is about 3–10 nm in maximum for XPS and about 2000 nm for Attenuated Reflection Mode (ATR) FTIR. In addition, the weak C=O band is located at lower wavenumbers (about 1700 cm^{-1}) than the vibration due to C=O of the carboxylic group originating from the acrylic acid comonomer. This result confirms that aldehyde groups are also formed, possibly as a result of auto-oxidation during exposure to air.

Furthermore, AAl shows an intense O-H stretching band in the wavenumber range of 3600–3000 cm^{-1}. The intensity of this band decreases sharply with increasing acrylic acid concentration in the comonomer blend. This band is only clearly observed up to a concentration of 50:50. Furthermore, from the first addition of acrylic acid (25% AA and 75% AAl), this vibration is superimposed by a broad and flat O–H stretching band due to the COOH group of acrylic acid. This band is observed in the wavenumber range from 3600 to 2000 cm^{-1}.

Even for the lowest concentration of acrylic acid (25%) in the comonomer blend, a strong >C=O band appears in the spectrum at about 1720 cm^{-1}.

The spectra in the wavenumber range of the >C=O vibration of AA and AAl are enlarged in Figure 5 to visualise the change in wavenumber position of this band

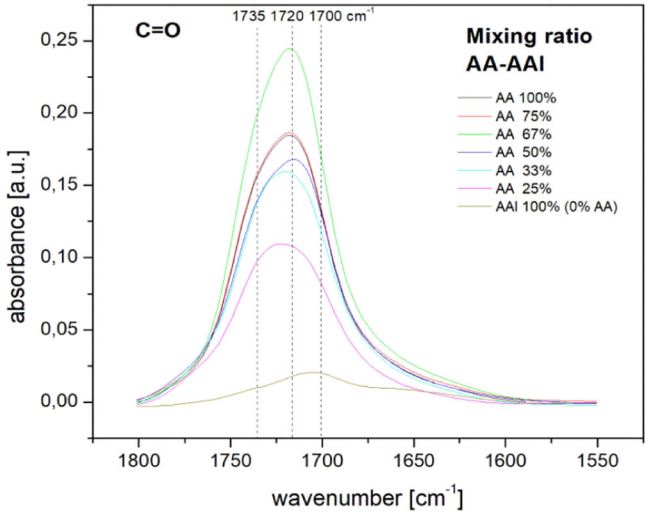

FIGURE 5 Carbonyl stretching vibration at 1700 cm^{-1} for different copolymers of AA and AAl.

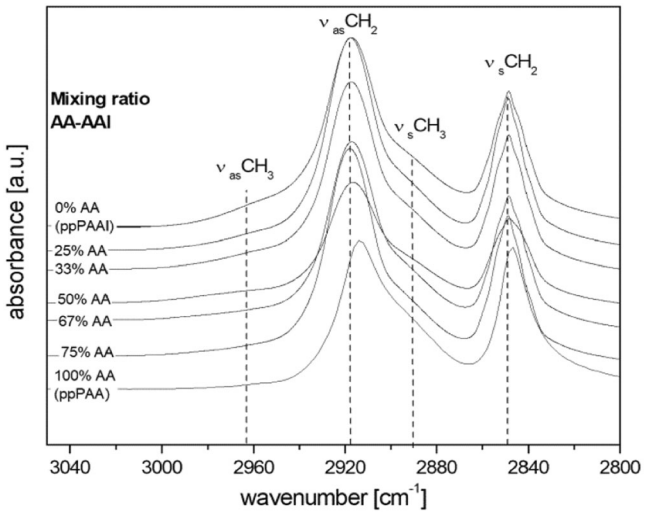

FIGURE 6 Stretching vibrations of CH_2 and CH_3 groups of copolymers deposited from allyl alcohol and acrylic acid in the wavenumbers range of 3050–2800 cm^{-1}.

with composition. The relative absorbance of the sample depends on the thickness of the deposited copolymer layers, because the maximum information depth of the diamond ATR of about 1000–2000 nm (depending on the wavenumber) is much larger than the thickness of the deposited copolymer layers. Therefore, this quantity cannot be interpreted scientifically.

The spectra of pure poly (allyl alcohol) also show a shoulder at $\nu \approx 1640-1630\ cm^{-1}$. Here the vibrations of the C=C double bonds are located in the IR signal. It can be speculated that a release of CO or H_2O during plasma exposure is responsible for the formation of new double bonds or for the binding without using the allyl double bond. As previously discussed, the formation of aliphatic esters by self-condensation of the acrylic acid may be responsible for the appearance of the shoulder at $\nu \approx 1730\ cm^{-1}$ as labelled in Figure 5. As already mentioned, esterification of allyl alcohol and acrylic acid is possible on exposure to plasma or during labelling with the aid of the carbodiimide used. In this case the water is quickly removed by the vacuum or chemically by the carbodiimide.

In summary, it can be concluded that AA and AAl can be bonded together by hydrogen bonding (AAl-OH... HOOC-AA), esterification (AAl-O-CO-AA) and copolymerisation (AAl-AA). It is also noted that the XPS and ATR-FTIR results are in good agreement and give some details of the reaction and side reactions.

The existence of some chain scissions is evidenced by the appearance of CH_3 groups in the IR spectra, indicating chain termination or side groups. This is evidenced by the appearance of a $\nu_{as}CH_3$ band at about $\nu \approx 2965\ cm^{-1}$. This band becomes more visible with increasing concentration of acrylic acid (Figure 6). A variety of different reactions are responsible for the formation of copolymer deposits with the aid of pulsed high frequency plasma.[15] As mentioned above, copolymerisation can occur in two different ways besides homopolymerisation:

- chemical copolymerisation
- random plasma specific copolymerisation
- separate homopolymerisation of allyl alcohol and acrylic acid
- side reactions such as self-condensation, esterification, etc.

Chemical copolymerisation obeys the chemical rules of copolymerisation, taking into account the copolymerisation parameters. Only true comonomers chemically polymerise into copolymers if the copolymerisation parameters allow it. It should be noted that the validity of such a copolymerisation mechanism under vacuum conditions is not proven. For example, the timely supply of comonomer molecules to the active chain centres is not guaranteed. Moreover, the theoretical approaches to copolymerisation are associated with reactions in solvents under atmospheric pressure conditions. These conditions are different from vacuum conditions. Random plasma copolymerisation is based on the fragmentation and/or atomisation of the comonomers. This wide variety of fragments and atoms leads to a significant contribution of randomly polymerised products through a variety of radical recombination during the deposition of the overall plasma copolymer. The characteristic of such polymer or copolymer layers is the absence of regular chemical structures. However, the chemically polymerised quantities are downgraded to irregular

structures when exposed to the high-energy vacuum UV radiation during plasma polymerisation.

In addition, some of the functional groups are cleaved, lost or rearranged. Another characteristic of plasma polymerisation is the presence of trapped radicals that can undergo auto-oxidation when the sample is exposed to ambient oxygen. The variety of auto-oxidative products is broad and includes all possible oxygen-containing functional groups (see Figure 7).[25] The fragmentation of the comonomers is also reflected in the release of hydrogen, a common process in plasma polymerisation.[25] Such excess hydrogen in the plasma atmosphere leads to the formation of CH_3 groups, which are easily identified by their asymmetric stretching vibration at $\nu \approx 2965\,cm^{-1}$ (Figure 6) in FTIR. Such methyl groups indicate the end of a growing chain and also the presence of side chains. Homopolymerisation is favoured by acrylic acid because the C=C double bond is very reactive. On the contrary, the double bond of allyl monomers tends to degradative chain transfer, resulting in inhibition of chain growth polymerisation.[14] It is therefore possible that the homopolymerisation of acrylic acid dominates (Figure 7) (Scheme 1).

In addition, acrylic acid can also self-condensate to anhydride, including 6- or 5-membered rings, which can be included in the copolymerisation process (Scheme 1). These processes are associated with the release of water. It has also been mentioned that acrylic acid can release CO_2. Allyl alcohol can also split off H_2O and form an oxygen-free fragment with a double bond. Decarbonylation should also be possible. Other photodegradation products of poly (vinyl alcohol), which may be comparable to poly (allyl alcohol), are aldehydes and carboxylic groups, both indicating chain scission of the polymer/copolymer (Scheme 1).[26] Figure 5 shows three possible carbonyl components of plasma polymerised pure allyl alcohol associated with aldehyde, carboxylic and ketone groups.[27]

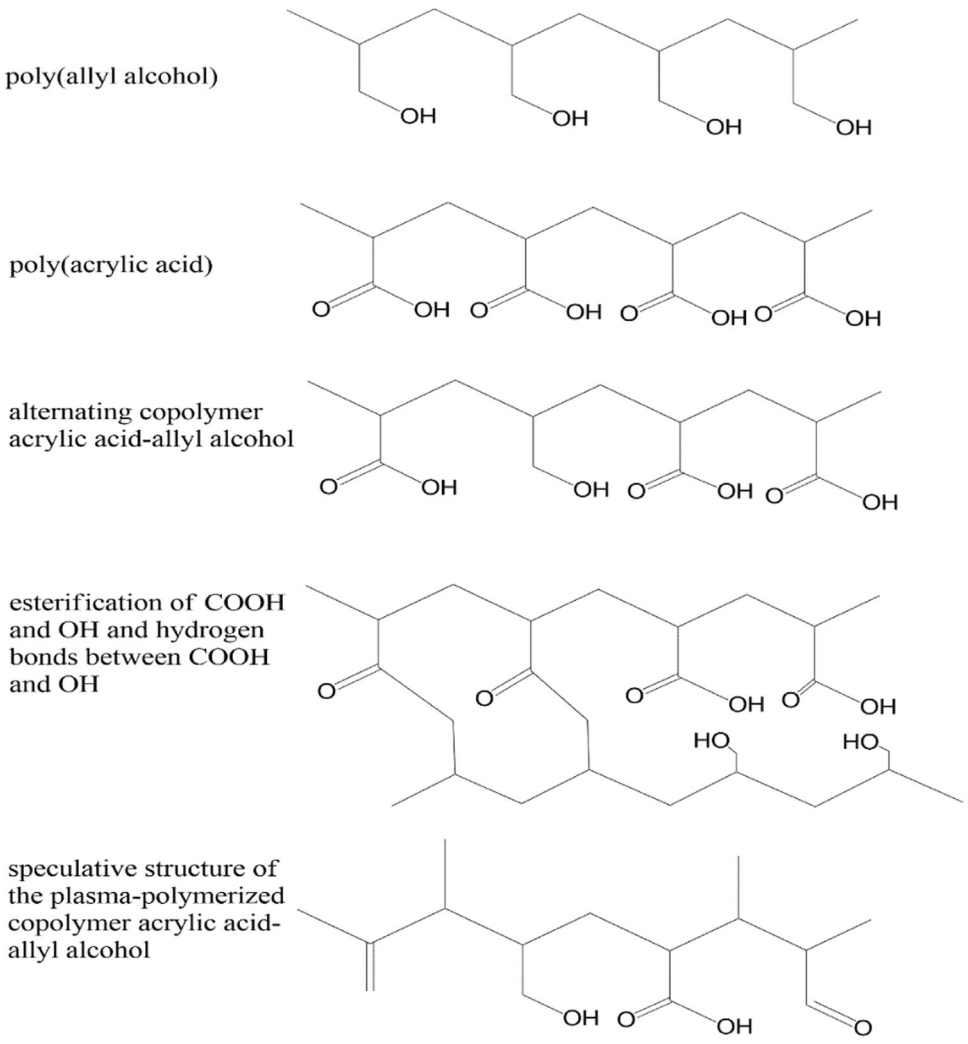

FIGURE 7 Homopolymers, copolymers, interaction and speculative structure of acrylic acid-allyl alcohol copolymers.

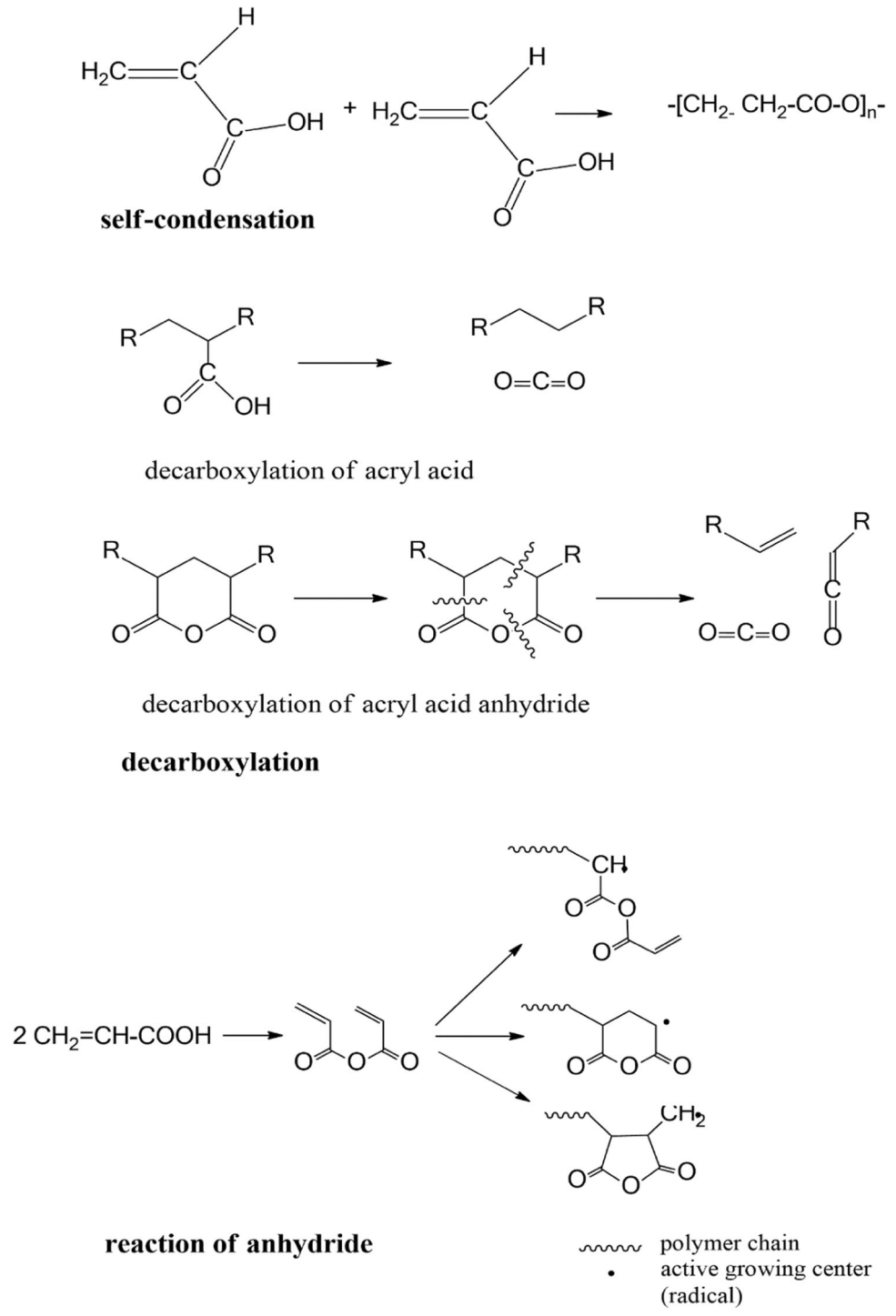

SCHEME 1 Side reactions of the acrylic acid-allyl alcohol system.

3.4 | Contact angle measurements

Water contact angles give an overview of the effect of all polar groups (−OH and −COOH) on the copolymer surface. The problem with all water contact angle measurements is that the copolymer can be partially dissolved by the water drop, as both poly (acrylic acid) and poly (allyl alcohol) are soluble in water. The composition of the drop is no longer pure water and is not constant over time. However, complete dissolution is hindered by components formed by plasma-induced cross-linking processes. This resistance to dissolution by water may be an indication of chemical bonding to a carbon backbone formed during the copolymerisation process.

It is surprising that pure plasma polymerised PAA does not have the lowest contact angle, whereas pure

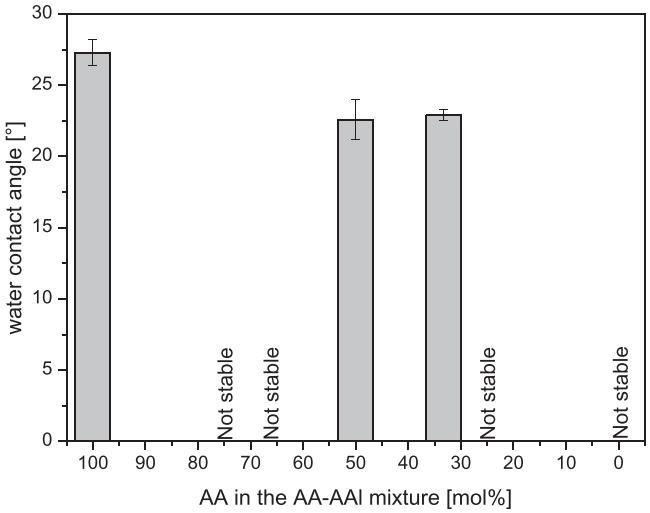

FIGURE 8 Water contact angles of the copolymer films from allyl alcohol and acrylic acid for the different formulated compositions.

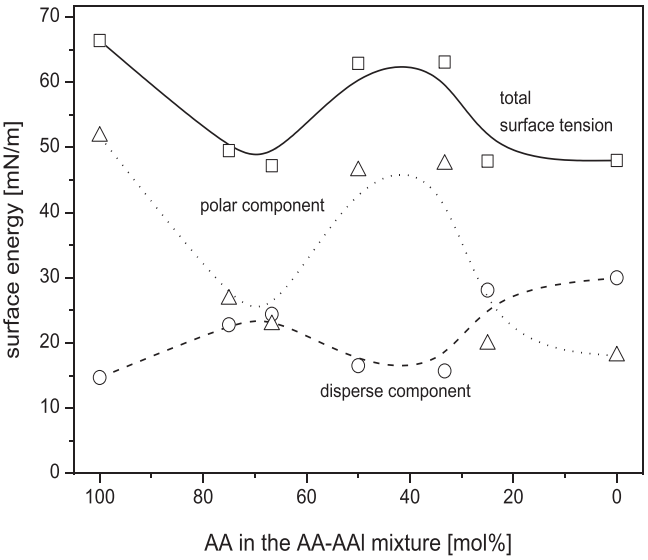

FIGURE 9 Free surface energy of the copolymers of acrylic acid and allyl alcohol as determined by the method of Fowkes, Owens, Wendt and Rabel.

PAAl was dissolved by water (Figure 8). This behaviour can be explained by the decarboxylation and subsequent cross-linking with a significant loss of COOH groups. Pure plasma deposited PAAl was soluble, meaning that the chemical structure has some linear sequences, oligomers and only a weak degree of cross-linking. Successfully measured copolymers must be cross-linked and should have a minority of soluble sequences.

Other test liquids were used to determine the surface energy (surface tension). In these experiments, the non-polar test liquids cannot dissolve the copolymer samples. Pure acrylic acid and the copolymer with 33% and 50% acrylic acid have the highest surface energy. The dispersive component is the lowest for pure acrylic acid, about 50% of that of poly (allyl alcohol) (Figure 9). Therefore, it can be concluded that pure acrylic acid and the copolymer with 33% and 50% acrylic acid are preferable for pH sensing applications.

3.5 | Broadband dielectric spectroscopy

The molecular mobility of the samples was investigated using BDS to measure the complex dielectric function isothermally for different temperatures. The samples were heated from 183 to 473 K and then cooled to 183 K. The dielectric loss as a function of both frequency and temperature is plotted in Figure 10 in a 3D representation for the copolymer of 75% AA during the cooling cycle. Some key dielectric features can be identified in the 3D plot. First, a broad peak in dielectric loss is observed at low temperatures, termed the α-relaxation. It should be noted that this process is referred to as

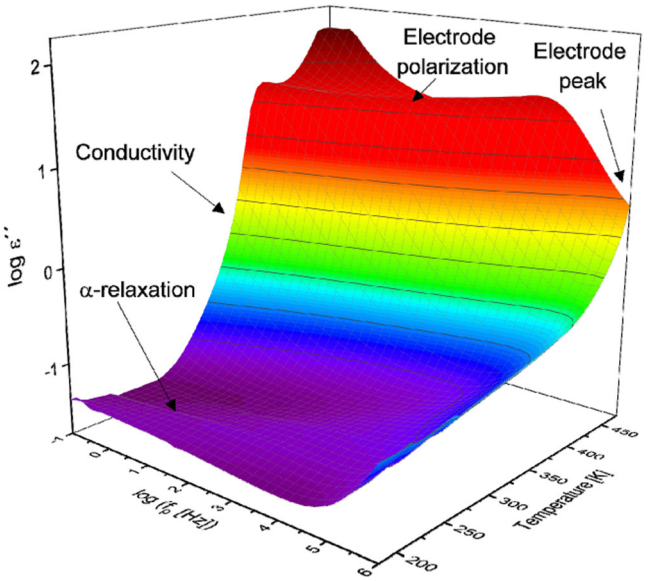

FIGURE 10 Dielectric loss as a function of frequency and temperature in a 3D representation during the cooling run of the 75% AA copolymer.

β-relaxation in ref.[25] Here, this process is assigned to α-relaxation for reasons discussed below.

The α-relaxation is attributed to segmental fluctuations in the copolymer. At temperatures higher than those relevant for α-relaxation, another peak is found in the dielectric loss. This peak was assigned to the electrode peak. This parasitic process is due to the thin film geometry of the system, where the resistance of the Al electrodes cannot be neglected.[26] Finally, a sharp increase in dielectric loss was

observed at low frequencies and high temperatures, due to the electrical conductivity of the sample and electrode polarisation effects. Conductivity is due to charge carriers such as ionic impurities remaining from sample preparation steps or ions resulting from the plasma process. Electrode polarisation is a parasitic effect due to the blocking of carriers at the electrodes. Figure 11 shows the dielectric loss of the same sample as in Figure 10 for a fixed frequency of $f = 103$ Hz as a function of temperature for both heating and cooling. There is a larger difference between the first heating and the first cooling. The first heating run was performed to erase the thermal history in all samples, including possible post-plasma reactions that take place at higher temperatures, such as radical recombination. Therefore, only the data from the cooling run were used for analysis.

The dielectric loss data have been plotted in the frequency domain for selected temperatures for the AA 25% sample in Figure S1 in the Supporting Information. With increasing temperature, the peak due to α-relaxation shifts to higher temperatures, as is characteristic of a relaxation process. The Havriliak-Negami (HN) function, given

$$\varepsilon_{HN}(\omega) = \varepsilon_\infty + \frac{\Delta\varepsilon}{(1 + (i\omega\tau_{HN})^\beta)^\gamma}, \quad (2)$$

was fitted to the data to analyze spectra quantitatively in the temperature range of 473–173 K for the first cooling cycle. Here, $\varepsilon_\infty = \lim_{\omega\to\infty} \varepsilon'(\omega)$, $\Delta\varepsilon$ is the dielectric strength and τ_{HN} is a characteristic relaxation time. β and γ are fractional shape parameters ($0 < \beta \leq 1$ and $0 < \beta\gamma \leq 1$) that describe the broadening and asymmetry of the relaxation peak with respect to the Debye function.[28] ω is the radial frequency ($\omega = 2\pi f$). Contributions related to conductivity were treated by adding $\frac{\sigma_0}{(\omega^s\varepsilon_0)}$ to the loss part of the HN-function. σ_0 is related to the DC conductivity and s is a parameter describing non-ohmic effects in the conductivity ($0 < s <= 1$). For thin film capacitors, the resistance of the aluminium electrodes cannot be ignored. It leads to an artificial loss contribution (electrode peak) to the dielectric loss on the high frequency side of the spectra. The electrode peak is accounted for by the first part of a mathematical Tayler series expansion of the Debye function as described in ref.[10,29] To reduce the number of free fit parameters, γ was fixed to one (symmetric relaxation spectra). An example of the fits is given in Supporting Information Figure.

The maximum of the dielectric loss was taken from the fit, denoted as the relaxation rate f_p. Log f_p is then plotted against inverse temperature as shown in the relaxation map in Figure 12 for the different monomer ratios. The plot shows that the temperature dependence of the relaxation rates is not linear, but curved in the Arrhenius diagram for the highest concentrations of AAl, as expected for α-relaxation. This temperature dependence can be described by the Vogel-Fulcher-Tammann (VFT) equation.[29–31]

$$f_p(T) = \frac{1}{2\pi\tau(T)} = f_\infty \exp\left(\frac{-A}{T - T_0}\right), \quad (3a)$$

f_∞ is a pre-exponential factor ($f_\infty \approx 10^{10}$–10^{12} Hz), T0 is the Vogel temperature or ideal glass transition temperature, which is found to be 40–70 K below the glass

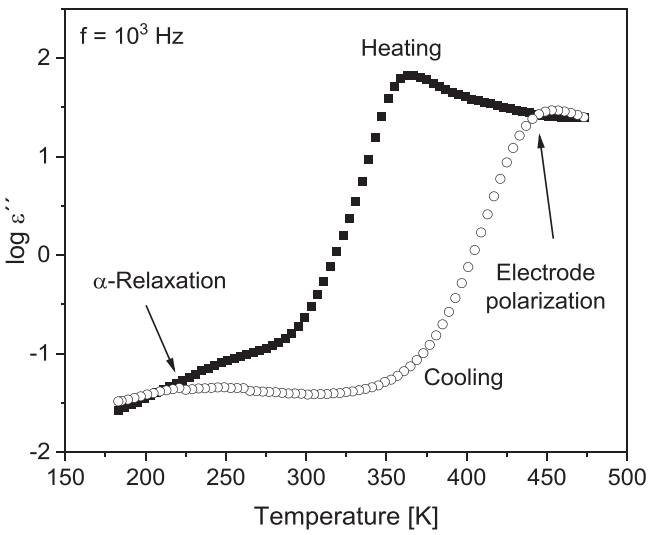

FIGURE 11 The dielectric loss log ε″ as a function of temperature during heating and cooling for the sample with formulated monomer composition AA 75%.

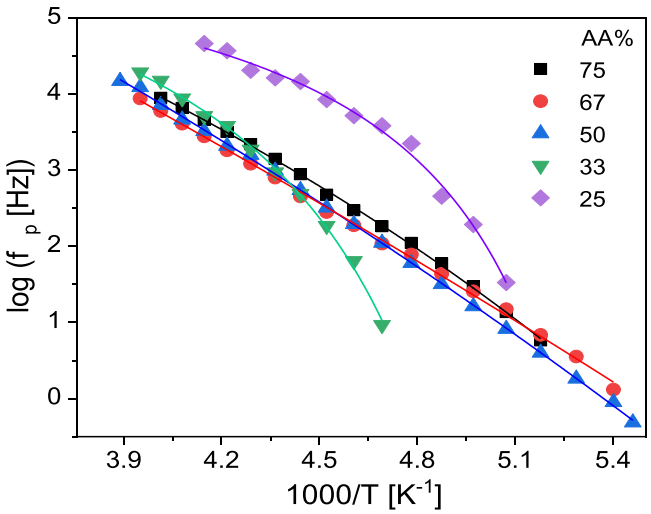

FIGURE 12 The relaxation map for all copolymer samples (black squares—75%, red circles—67%, blue triangles up—AA 50%, green triangles down—AA 33%, and purple diamonds—AA 25%). The solid lines are VFT (Vogel-Fulcher-Tammann) fits for each copolymer.

transition temperature measured by DSC, and A is a constant. The curved temperature dependence of the relaxation rates indicates that the α-relaxation is related to the glass transition.

For lower concentrations of AAl, the temperature dependence of the relaxation rates appears to be less curved and could be described by the Arrhenius equation, which reads

$$f_p(T) = \frac{1}{2\pi\tau(T)} = f_\infty \exp\left(\frac{-E_A}{RT}\right). \quad (4a)$$

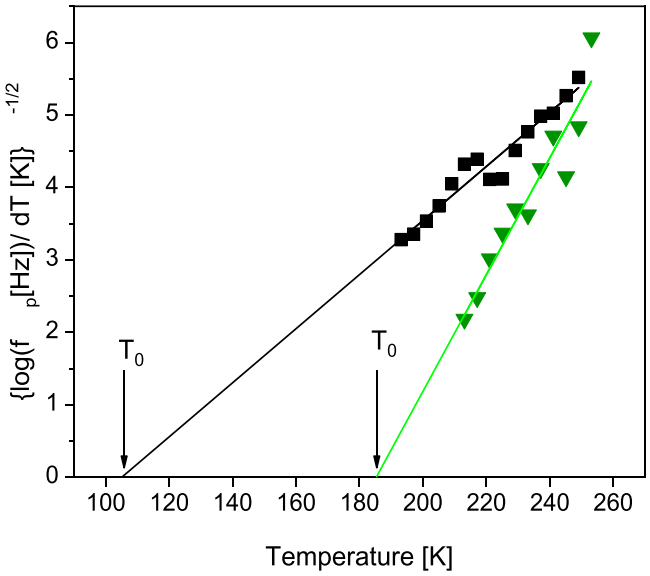

FIGURE 13 The derivative of the relaxation rate according to Equation (3b) for the copolymers AA 33%, (green triangles) and AA 75%, (black squares). Lines are linear regressions to the corresponding data.

Where EA is the (apparent) activation energy and R is the general gas constant. A derivative approach can be used to distinguish between Arrhenius and VFT dependence, independent of the pre-factor. For the VFT dependence this approach gives

$$\left(\frac{dlogf_p}{dT}\right)^{-1/2} = A^{\frac{-1}{2}}(T - T_0). \quad (3b)$$

Equation 3b defines a straight line. For $(dlog\ f_p/dT)^{-1/2} = 0$ the Vogel temperature T_0 can be obtained. The derivative approach also gives a straight line for the Arrhenius equation[32]

$$\left(\frac{dlogf_p}{dT}\right)^{-1/2} = \left(\frac{2.3R}{E_A}\right)^{1/2} T, \quad (4b)$$

but through the point of origin. Figure 13 plots $(dlog\ f_p/dT)^{-1/2}$ versus temperature for the copolymers with the formulated concentrations AA 33% and AA 75%. The derivative analysis shows that the temperature dependence of the relaxation also has a VFT-like temperature dependence for the highest concentrations of AA. However, the change in the temperature dependence of the relaxation rate from a more curved to a less curved dependence with decreasing AAl concentration may indicate a change in the structure of the plasma deposited copolymers.

From the derivative approach the Vogel temperature T_0 is derived (see Figure 13) and plotted against the concentration of acrylic acid in Figure 14. For the lowest concentration of AA (33% AA), T_0 is approximately

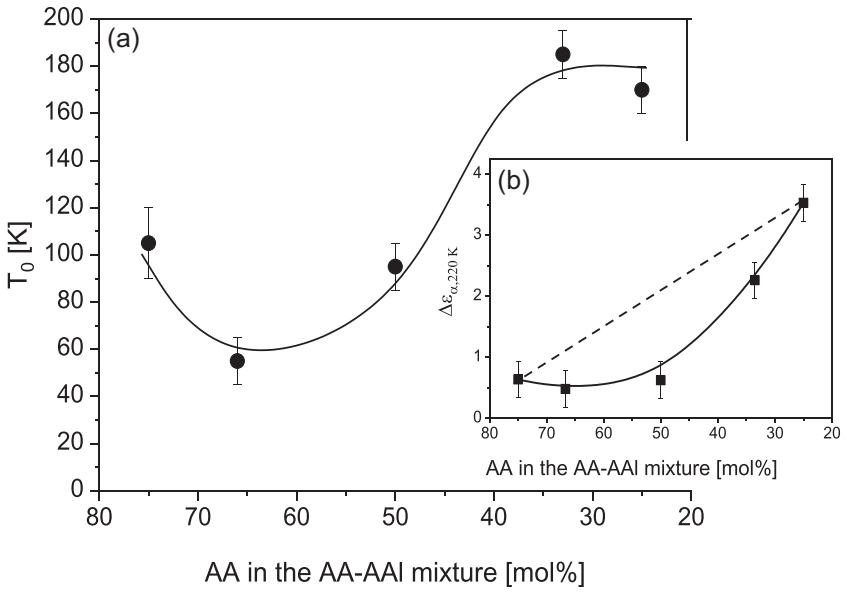

FIGURE 14 Vogel temperature T_0 versus the concentration of acrylic acid. The line is a guide to the eyes. The inset depicts the relaxation strength of the α-relaxation $\Delta_{\alpha,220\ K}$ taken at 220 K versus the concentration of acrylic acid. The solid line is a guide to the eyes. The dotted line represents the one-to-one dependence.

constant, while for higher concentrations it decreases with a minimum between 60% and 70% AA. This behaviour, as discussed above for the deposition rate, could indicate a true copolymerisation.

The dielectric strength α-relaxation ($\Delta\varepsilon_\alpha$) obtained from the HN is plotted as a function of temperature for the AA 75% copolymers in Figure S3 in the Supporting Information. $\Delta\varepsilon_\alpha$ decreases with increasing temperature, as is typical for α relaxation.[20] The temperature dependence of $\Delta\varepsilon_\alpha$ seems to be stronger for AA 25% than that for AA 75%.

The inset of Figure 14 shows the concentration dependence of the dielectric constant of the α-relaxation taken at 220 K $\Delta\varepsilon_{\alpha,220\,K}$. $\Delta\varepsilon_{\alpha,220\,K}$ decreases with increasing concentration of AA. The decrease in $\Delta\varepsilon_{\alpha,220\,K}$ is due to the higher dipole moment of AAl compared to AA. A linear relationship would be expected for a true alternating copolymerisation. The inset of Figure 14 shows that the experimental dependence is much stronger for low concentrations of AA. This result may indicate that no true copolymerisation takes place at low concentrations of acrylic acid. A plateau is observed at concentrations of around 50 mol% AA. This behaviour could again indicate true copolymerisation.

From the complex dielectric function, the complex conductivity σ*(ω) can be calculated by

$$\sigma^*(\omega) = \sigma'(\omega) - i\sigma''(\omega) = i\omega\varepsilon_0\varepsilon^*(\omega), \quad (5)$$

σ'and σ″ denote the real and the imaginary part of the complex conductivity, respectively where ε_0 is the permittivity of vacuum.[33] Figure S4 in the Supporting Information shows the real part of the complex conductivity for the nominal concentrations of AA 75% and AA 25%. In principle, the conductivity spectra show the frequency dependence expected for a semiconducting soft matter material.[21] At high frequencies $\sigma'(f)$ decreases with decreasing frequency according to a power law until reaching a plateau value at a critical frequency f_c. The plateau value is due to the DC conductivity σ_{DC}. The further decrease of the real part of the complex conductivity is due to the strong electrode polarisation effects which complicate the quantitative analysis of the conductivity spectra. Nevertheless $\sigma'(f)$ was analyzed by the well-known Jonscher law[34] which reads

$$\sigma'(f) = \sigma_{DC}\left(1 + \left(\frac{f}{f_c}\right)^n\right). \quad (6)$$

Here, σ_{DC} is the DC conductivity, n is an exponent with values between 0.5 and 1. The Jonscher formula is fitted to the conductivity spectra with the data affected by electrode polarisation excluded from the fit. It should be noted that the *σ_DC* values are subject to larger errors due to electrode polarisation.

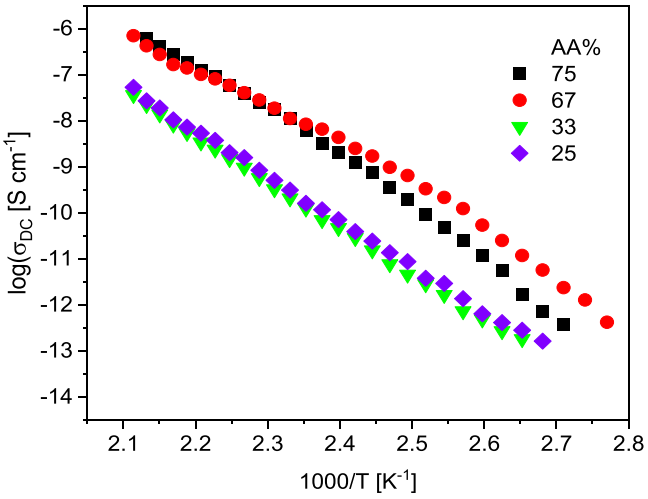

FIGURE 15 DC conductivity versus reciprocal temperature at the indicated compositions.

The DC conductivity is plotted against the inverse of the temperature as shown in Figure 15 for all the compositions studied. Like the relaxation rates shown in Figure 12, the temperature of the *σ_DC* groups has two different dependencies. For low concentrations of AA, the dc conductivity is about 1.5 orders of magnitude higher than for high concentrations. In addition, the temperature dependence of *σ_DC* seems to be more curved for low concentrations of acrylic acid than for higher ones. Again, this behaviour can be discussed as a transition from homopolymerisation (high AA concentration) to copolymerisation (low AA concentration).

4 | CONCLUSIONS

The plasma-induced copolymerisation of acrylic acid and allyl alcohol films has been developed as a new route for pH sensing applications. The structure-property relationship of these copolymers was discussed as a function of the molar ratio of AA and AAl comonomers. H-bonding and condensation processes play an important role in the concentration dependence of the deposition rate as well as the structure of the copolymers. Pure acrylic acid and the copolymers with 33% and 50% acrylic acid were found in a partially cross-linked form with a significant loss of –COOH groups. These polymers are therefore preferred for pH sensing applications. The results obtained from the BDS measurements indicate that no true copolymerisation takes place at low concentrations

of acrylic acid. At concentrations of around 50% AA a plateau in the $\Delta\varepsilon_\alpha$ value is observed. This behaviour could be indicative of true copolymerisation. In addition, for low concentrations of AA the DC conductivity is about 1.5 orders of magnitude higher than for high concentrations and the temperature dependence of σ_DC, when plotted against 1/T, looks more curved for low concentrations of AA compared to higher ones. The transition from homopolymerisation (high AA concentration) to copolymerisation (low AA concentration) could be the reason for this behaviour.

ACKNOWLEDGMENTS

Open Access funding enabled and organized by Projekt DEAL.

CONFLICT OF INTEREST STATEMENT

The authors declare no conflicts of interest.

DATA AVAILABILITY STATEMENT

The data that support the findings of this study are available from the corresponding author upon reasonable request.

ORCID

Alaa Fahmy http://orcid.org/0000-0002-9060-0135

REFERENCES

[1] S. Cichosz, A. Masek, M. Zaborski, *Polym. Test.* **2018**, *67*, 342.
[2] N. Fomina, C. A. Johnson, A. Maruniak, S. Bahrampour, C. Lang, R. W. Davis, S. Kavusi, H. Ahmad, *Lab Chip* **2016**, *16*, 2236.
[3] Q. Thong Trinh, G. Gerlach, J. Sorber, K. F. Arndt, *Sens. Actuators, B* **2006**, *117*, 17.
[4] E. A. Kamoun, A. Fahmy, T. H. Taha, E. M. El-Fakharany, M. Makram, H. M. A. Soliman, H. Shehata, *Int. J. Biol. Macromol.* **2018**, *106*, 158.
[5] O. Korostynska, K. Arshak, E. Gill, A. Arshak, *Sensors* **2007**, *7*, 3027.
[6] P. Rivolo, M. Castellino, F. Frascella, S. Ricciardi, Life Sciences, *Open Access Book*, Intech, Rijeka, HR **2015**.
[7] M. J. Hawker, A. Pegalajar-Jurado, K. I. Hicks, J. C. Shearer, E. R. Fisher, *Plasma Processes Polym.* **2015**, *12*, 1435.
[8] A. Fahmy, T. A. Mohamed, J. F. Friedrich, *Appl. Surf. Sci.* **2018**, *458*, 1006.
[9] M. I. Khan, K. Mukherjee, R. Shoukat, H. Dong, *Microsyst. Technol*, Springer, Berlin-Heidelberg **2017**, https://doi.org/10.1007/s00542-017-3495-5
[10] J. F. Friedrich, R. Mix, G. Kühn, *Surf. Coat. Technol.* **2003**, *174-175*, 811.
[11] A. Fahmy, R. Mix, A. Schönhals, J. Friedrich, *Plasma Processes Polym.* **2013**, *10*, 750.
[12] E. Ruckenstein, L. Liang, *JAPS* **1996**, *62*(7), 973.
[13] J. Zeng, H. Hou, J. H. Wendorff, *e-Polymers* **2004**, *78*, 8.
[14] H. G. Elias, *Makromoleküle*, Hüthig & Wepf, Basel, CH, **1990**.
[15] A. Fahmy, A. El-Zomrawy, A. M. Saeed, A. Z. Sayed, M. A. E. El-Arab, H. A. Shehata, J. Friedrich, *J. Adhes. Sci. Technol.* **2017**, *31*, 1422.
[16] H.-G. Elias, *An Introduction to Polymer Science*, VCH, Weinheim, Germany **1997**.
[17] J. Friedrich, *Plasma Processes Polym.* **2011**, *8*, 783.
[18] J. Friedrich, *Advanced Techniques for Surface Design*, Wiley-VCH, Weinheim **2012**.
[19] A. Fahmy, R. Mix, A. Schönhals, J. F. Friedrich, *Plasma Chem. Plasma Process.* **2011**, *31*, 477.
[20] A. Fahmy, R. Mix, A. Schönhals, J. F. Friedrich, *Plasma Processes Polym.* **2011**, *8*, 147.
[21] A. Fahmy, J. Friedrich, *J. Adhes. Sci. Technol.* **2013**, *27*, 324.
[22] A. Schönhals, F. Kremer *Theory of dielectric relaxation in Broadband Dielectric Spectroscopy*, (Eds. F. Kremer, A. Schönhals), Springer, Berlin **2002**, pp. 1 2002.
[23] A. Fahmy, A. Schönhals, *Plasma Processes Polym.* **2016**, *13*, 499.
[24] A. Fahmy, A. Schönhals, J. Friedrich, *J. Phys. Chem. B* **2013**, *117*, 10603.
[25] A. Fahmy, J. Friedrich, F. Poncin-Epaillard, D. Debarnot, *Thin Solid Films* **2016**, *616*, 339.
[26] A. Fahmy, L. A. Jácomeb, A. Schönhals, *Journal of Physical Chemistry: C* **2020**, *124*, 22817.
[27] J. Friedrich, G. Kühn, J. Gähde, *Acta Polym.* **1979**, *30*, 470.
[28] H. Yin, S. Napolitano, A. Schönhals, *Macromolecules* **1652**, *2012*, 45.
[29] H. Vogel, *Phys. Z.* **1921**, *22*, 645.
[30] A. Schönhals, F. Kremer *Analysis of dielectric spectra in Broadband Dielectric Spectroscopy*, 59 (Eds. F. Kremer, A. Schönhals), Springer, Berlin **2002**, pp. 2002.
[31] G. S. Fulcher, *J. Am. Ceram. Soc.* **1925**, *8*, 339.
[32] G. Tammann, W. Hesse, *Zeitschrift für anorganische und allgemeine Chemie* **1926**, *156*, 245.
[33] A. Fahmy, A. M. Saeed, U. Dawood, H. Abdelbary, K. Altmann, A. Schönhals, *Mater. Chem. Phys.* **2023**, *296*, 127277.
[34] A. K. Jonscher, *Nature* **1977**, *267*, 673.

SUPPORTING INFORMATION

Additional supporting information can be found online in the Supporting Information section at the end of this article.

How to cite this article: A. Fahmy, H. Omar, P. Szymoniak, A. Schönhals, J. F. Friedrich, *Plasma. Process. Polym.* **2023**, e2300071. https://doi.org/10.1002/ppap.202300071